J Physiol Sci (2011) 61:259–266
DOI 10.1007/s12576-011-0143-1

SHORT COMMUNICATION

Lateral diffusion of manganese in the rat brain determined by T_1 relaxation time measured by ^{1}H MRI

Yoshiteru Seo · Akira Takamata · Takashi Ogino · Hironobu Morita · Masataka Murakami

Received: 21 January 2011 / Accepted: 8 March 2011 / Published online: 26 March 2011

Abstract In order to optimize manganese ion-enhanced MRI in thalamic and hypothalamic nuclei, we analyzed the diffusion of manganese in the brain followed by the intra-cerebroventricular application of manganese-bicine (Mn-bicine). T_1-weighted MRI intensities, with 9-pixel ROIs in the hypothalamus perpendicular to the third ventricle, were measured during continuous infusion of Mn-bicine solution in the lateral cerebroventricle. Using a relationship between the image intensity of T_1-weighted MRI and T_1 relaxation time, the image intensity was converted into the concentration of manganese. Assuming a simple diffusion process, the apparent diffusion coefficient (D_{ap}) of manganese (4.2×10^{-5} mm^2 s^{-1}) is much lower than that of water (6×10^{-4} mm^2 s^{-1}), and the D_{ap} tended to decrease when the distance from the third ventricle increased. These results suggest (1) the Mn^{2+} ion is trapped by neural cells during diffusion and (2) the manganese efflux is discharged from the brain via veins.

Keywords Manganese · Brain · MnEMRI · Functional MRI · Mn-bicine

Introduction

Manganese ion-enhanced MRI (MnEMRI) [1] takes advantage of the higher sensitivity to detect neuronal activities in small regions or nuclei in the brain, such as the supraoptic nucleus of the rat [2, 3]. However, the cellular toxicity of Mn^{2+} is a major drawback to MnEMRI when it is administrated intravenously or intraperitoneally [4]. Therefore, focal injections of Mn^{2+} have been proposed to minimize the dosage of Mn^{2+}, such as intracerebroventricular injections or direct injections to the target region [5]. We are interested in the thalamic and hypothalamic functions, and intend to analyze the response of the supraoptic and paraventricular nuclei, etc. Since these nuclei are positioned near the third ventricle and the subarachnoidal space, the intracerebroventricular application of Mn^{2+} might be useful to detect these nuclei without any effect on other vital organs, such as the heart, liver, and kidneys. In addition, a low affinity chelate, Mn-bicine, has been used to minimize the toxic effects of Mn^{2+} [6]. When Mn-bicine is infused in the cerebrospinal fluid (CSF), manganese can transfer into the interstitial space of the

The experiments were carried out in the laboratory of Department of Nano-Structure Physiology, Center for Integrative Bioscience, National Institute for Physiological Sciences, Okazaki, Japan. Y.S., A.T., T.O, and H.M. contributed to the conception and design of the study. All authors contributed to the collection, analysis and interpretation of data, and also to the writing of the article and critical revisions. Then, all authors approved the final version of the manuscript.

Y. Seo (✉) · T. Ogino
Department of Regulatory Physiology,
Dokkyo Medical University School of Medicine, Tochigi, Japan
e-mail: yseo@dokkyomed.ac.jp

A. Takamata
Department of Environmental Health,
Nara Women's University, Nara, Japan

H. Morita
Department of Physiology,
Gifu University Graduate School of Medicine, Gifu, Japan

M. Murakami
Department of Nano-Structure Physiology, Center for Integrative Bioscience, National Institute for Physiological Sciences,
Okazaki, Japan

brain through the ependymal layer that covers the surface of the ventricle. In order to optimize this entry process, we have analyzed the diffusion process of manganese into the hypothalamus from the direction perpendicular to the third ventricle. Admittedly, the experimental conditions were complicated. Judging from the conditional association constant of Mn-bicine ($K_{a'} = 10^{2.9}\ M^{-1}$ at pH 7.4) [6], when 2 mM of the Mn-bicine solution was infused from the lateral ventricle of the rat brain, half of the manganese dissociated into free Mn^{2+}, and the remaining part bound with bicine. Since Mn-bicine and Mn^{2+} can pass the ependymal layer of the ventricles [7], and part of the Mn^{2+} may bind with citrate and bicarbonate in the interstitial fluid [8, 9], we have to consider the sum of diffusion of more than four types of manganese. In this text, "manganese" refers to all of these types. In addition, brain parenchyma is not a homogeneous fluid, but rather consists of several types of neural cells and tissue structures. Some amount of Mn^{2+} may enter into neural cells, and some amount of manganese efflux may be discharged via the veins. Therefore, the observed diffusional behavior and diffusion constant of the manganese should reflect these conditions and thus provide an approximation of the diffusion of manganese in the brain. Even considering the limitations of the study, this is the first attempt to analyze the diffusion of manganese inside the brain quantitatively.

Methods

Preparation of the rat for the MRI experiments

Male Wistar-Hamamatsu rats (b.w. 260–340 g) were initially anesthetized by enflurane inhalation. After a tracheal cannulation, anesthesia was changed to 1% enflurane in a gas mixture of 36% O_2/2% CO_2/62% N_2O delivered through a tracheal cannula by an artificial ventilator. An intraventricular cannula was inserted in the left lateral ventricle (1.5 mm left of the midline and 0.8 mm caudal to the bregma), and polyethylene tubing was connected with a syringe pump for injection of Mn-bicine saline solution. Then, anesthesia was switched from enflurane to α-chloralose (70 mg/kg b.w. i.p.), and ventilation was continued with O_2/CO_2 and N_2O. After the experiments, rats were euthanized by an overdose of anesthesia (pentobarbital, 500 mg/kg body weight i.v.). All of the animal experiments conducted in this study were carried out under the rules and regulations of the 'Guiding Principles for the Care and Use of Animals' stipulated by the Physiological Society of Japan. The experiments were approved by the Institutional Animal Care and Use Committee of the National Institute for Natural Sciences.

Acquisition of MR images

Rats were placed in the prone position on a custom-built Plexiglas sledge, and the position of the head was fixed with a pair of earplugs and a bite bar. A home-built ^1H RF surface coil (24 mm in diameter) was placed on the surface of the head. ^1H MR images were obtained by a 4.7-T animal imaging system (ABX-4.7/40, Bruker, Karlsruhe) with ParaVison operating software (version 2.1.1), and the system was equipped with an active shielded gradient (BGA-120, Bruker, Karlsruhe).

Six pairs of measurements of the four sets of T_1-weighted images and a set of T_1 relaxation times of the CSF and the brain were repeated before and during Mn-bicine infusion (0.1 μmol/h). Then, 36 sets of T_1-weighted images were obtained every 61 s. The typical imaging parameters used for the T_1-weighted gradient-echo imaging were as follows: 25 × 25 mm field of view (FOV), 128 × 128 data matrix, 1 mm slice thickness, 50.3 ms relaxation delay (TR), 4.2 ms echo-time (TE), 5 slices, 8 accumulations, and the 61-s image acquisition interval. A sinc-shaped pulse (duration 2 ms, with a bandwidth 2.5 kHz) was used for excitation. The RF power was adjusted as a 180° pulse in the center of the coil, which roughly corresponded to a 90° pulse at the depth of the lateral ventricles of the rats.

T_1 relaxation time was measured using an inversion-recovery fast-imaging sequence employing a single 180° pulse prior to the acquisition of a series of low flip-angle detection pulses (FLASH). The parameters used were as follows: 25 × 25 mm FOV, 128 × 128 data matrix, 1 mm slice thickness, 1 slice, and 2 accumulations. An adiabatic pulse (4 ms duration, 2.5 kHz bandwidth) was used for inversion. The RF power was adjusted as a 180° pulse in the depth of the lateral ventricles of the rats. A series of eight sinc-shaped RF pulses (20° flip angle ca., 2 ms duration, and 2.5 kHz bandwidth) was used for detection. Five inversion recovery delays (TI, 45–5000 ms) were used for the T_1 measurements [10].

In separate experiments, the ventricular system was visualized by 3D gradient-echo imaging with the following parameters: 25 × 25 × 25 mm FOV, 128 × 128 × 64 data matrix, 100 ms TR, 3.2 ms TE, and 2 accumulations. A block pulse (duration 0.2 ms) was used for excitation, and intraventricular infusion of Gd-DTPA was continued (0.25 μmol/h) during the measurements. 3D reconstruction was performed after the data matrix was interpolated to 256 × 256 × 256. The diffusion coefficient of water in the hypothalamus was measured by spin-echo pulse-field gradient imaging with the following parameters: 25 × 25 mm FOV, 128 × 128 data matrix, 1 mm slice thickness, 9 slices, and 2 accumulations. The time interval between the gradient pair (Δ) and duration of the gradient pulse (δ)

were 26 ms and 6 ms, respectively. The direction of the diffusion pulse was set so it was perpendicular to the third ventricle. The diffusion coefficient was calculated from *b* values ranged from 20 to 1400 mm^{-2} s obtained from four images.

Model and data analysis of diffusion of manganese

The third ventricle (3V) in the rat has a unique structure. As shown in Fig. 1, the lateral ventricles are connected to the 3V by the interventricular foramina. The upper part of 3V continues caudally to the aqueduct. The lower part of the 3V goes down the anterior side of the thalamus, then makes a thin slit between the hypothalamus, and finally climbs up the posterior side of the thalamus to join the aqueduct to the fourth ventricle (4V). As reported previously [11], CSF may flow from the lateral ventricles to the 3V, then continue on to the aqueduct and the 4V. We may expect a caudal flow of the CSF in the thin part of the 3V, so the Mn-bicine concentration in the 3V was kept at a constant level. Because the thin part of the 3V is more than 3 mm in length and 1.5 mm in height, it is large enough, compared with the voxel size (195 × 195 × 1000 μm), positioned parallel to the 3V (Fig. 1a–c). Therefore, we treated the manganese diffusion as a one-dimensional simple diffusion perpendicular to the 3V. A series of ROIs (9 pixels) was set from the thin part of the 3V to the area perpendicular to the 3V, as shown in Fig. 1d.

The inner surface of the ventricle is covered with a single layer of ependymal cells. The ependymal epithelium is considered to be leaky, with a permeability higher than that of the capillaries of the choroid plexus [7]. When Mn-bicine was injected intravenously, it quickly appeared in the CSF (unpublished result). Therefore, not only Mn-citrate (245 Da), but also Mn-bicine (216 Da) may pass the capillary endothelium of the choroid plexus. Therefore, it might be true that Mn-bicine also passes through the ependymal epithelium from the CSF to the interstitial space of the brain.

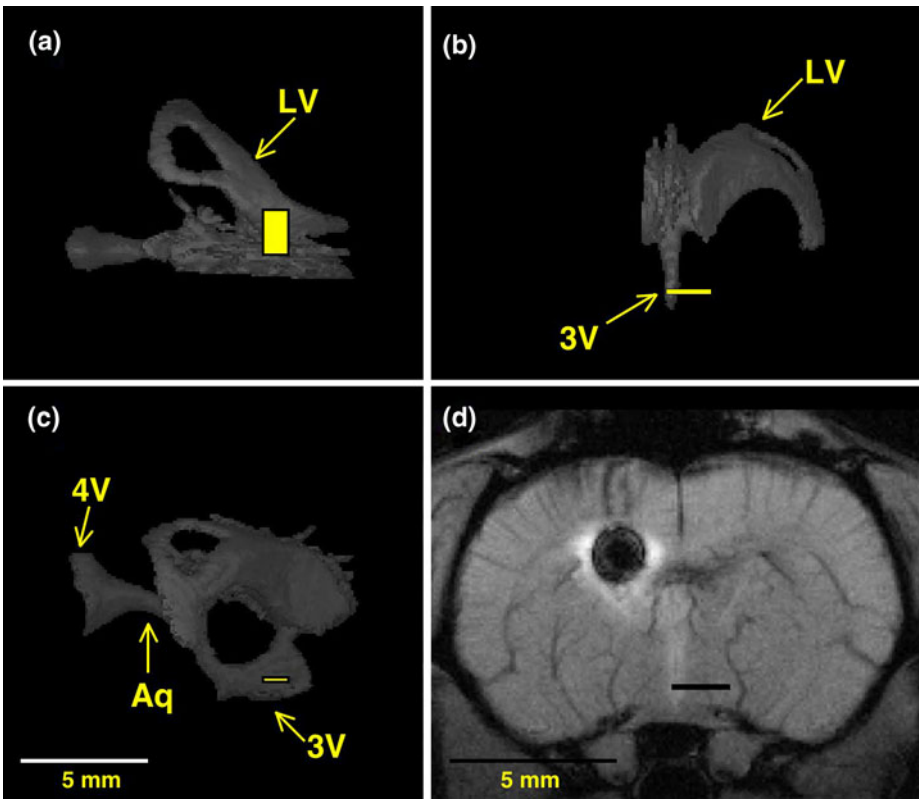

Fig. 1 The three-dimensional structure of the rat ventricular system and the ROI used for the measurement of manganese diffusion. **a**, **b**, **c** show dorsal (**a**), frontal (**b**), and lateral (**c**) views of the right half of the ventricular system. Ventricles are depicted by 3D gradient-echo images obtained during the ventricular infusion of Gd-DTPA. The three *boxes* indicate the position and size of the ROI shown in **d**. **d** A T_1-weighted coronal gradient-echo image of a rat brain at 1 mm caudal to the bregma. The artifact (*black round shape*) in the image, in the left ventricle, is the tip of the injection cannula. Since Mn-bicine had already been injected, the CSF in the ventricle was depicted as a high intensity. The *black horizontal bar* represents the ROI, 9 pixels (195 × 1758 μm), perpendicular to the 3rd ventricle, used to measure Mn^{2+} diffusion. The abbreviations used are as follows: *LV* left side of the lateral ventricle, *3V* the third ventricle, *Aq* the ventricular aqueduct, and *4V* the fourth ventricle

The simple diffusion equation is given by

$$\partial C/\partial t - D_{ap} \cdot \partial^2 C/\partial x^2 = 0, \quad (1)$$

where C is the total manganese concentration, including Mn^{2+}, Mn-bicine, and Mn-citrate, etc. D_{ap} is the apparent diffusion coefficient of manganese, and x is the distance from the 3V. Based on the assumption of the initial conditions: $C(x,0) = 0$, and boundary conditions: $C(0,t) =$ Co and $C(\infty,t) = 0$, the manganese concentration is given by

$$C(x,t) = \mathrm{Co} \cdot \mathrm{erfc}[x/(2(D_{ap} \cdot t)^{0.5})]. \quad (2)$$

In the T_1-weighted imaging with a 90° excitation pulse and a short echo time, the observed signal intensity of the image ($M(x,t)$) reaches a steady value

$$M(x,t) = M_O[1 - \exp(-\mathrm{TR} \cdot R_1(x,t))], \quad (3)$$

where $R_1(x,t)$ is T_1 relaxation rate ($1/T_1$) of the brain, M_o is the equilibrium image intensity, and TR is the repetition time of the excitation pulse. The $R_1(x,t)$ is the sum of the intrinsic relaxation rate of brain (R_0) and the relaxation rate of the manganese (R_{Mn}), which is proportional to the manganese concentration ($C(x,t)$), and the relaxivity value of the manganese (K_1). Because of the relaxivity of Mn^{2+}, Mn-bicine and Mn-citrate were similar in saline solution (around 5 mM^{-1} s^{-1}); a single and constant K_1 value was supposed in this calculation. $R_1(x,t)$ is given by

$$R_1(x,t) = R_0 + R_{Mn} = R_0 + K_1 \cdot C(x,t). \quad (4)$$

Since the increase in the relaxation rate ($\Delta R_1(x,t) = R_1(x,t) - R_0$) is proportional to the manganese concentration, Eq. 2 can be written

$$\Delta R_1(x,t) = \Delta R_{10} \cdot \mathrm{erfc}[x/(2(D_{ap} \cdot t)^{0.5})], \quad (5)$$

where ΔR_{10} is $K_1 \cdot \mathrm{Co} - R_0$. Therefore, using Eqs. 2 and 5, we can obtain D_{ap} from the time-dependent changes of T_1-weighted image intensity ($M(x,t)$).

In Eq. 3, we assumed a uniform excitation pulse with a flip angle of 90° and an infinitely short TE. Since we used a surface coil for the imaging and finite length of TE (3.2 ms), these assumptions were not satisfied by the actual measurements. However, the measurement of T_1 relaxation time is time-consuming even using the inversion-recovery fast-imaging sequence, and we could not follow the initial part of the diffusion. As a practical method to overcome this difficulty, we measured the T_1 relaxation rates during the Mn-bicine infusion, and then, the values of the observed relaxation rate (R_{1ob}) and the image intensity (M_{ob}) were used in Eq. 3. Using this "calibration curve," $R_1(x,t)$ was estimated from $M(x,t)$.

Statistics and fitting

All numerical values were expressed as the mean and standard error of the mean (mean ± SE). One-way analysis of variance or Student's t test was employed for the statistical significance tests, and it was considered that p values less than 0.05 indicated significance. Linear and non-linear fittings were conducted using IGOR Pro (v4.0.9A, WaveMetrics, Oregon).

Results

Estimation of T_1-relaxation rate from image intensity of T_1-weighted GE image

The intensity of 9 pixels of the brain was measured during a continuous injection of 2 mM Mn-bicine at 50 µl/h. A typical result is shown in Fig. 2a. The image intensity of the 3V increased quickly and reached the peak at 5 min, then decreased gradually because of accumulation of Mn-bicine in the CSF. The image intensity of pixels near the 3V increased faster than those far from the 3V. In order to convert image intensity to T_1 relaxation rate, we applied a non-linear fitting of the T_1 relaxation rate (R_{1ob}) and T_1-weighted image intensity (M_{ob}) to an equation: $M_{ob} = M_O^*[1 - \exp(-\mathrm{TR}^* \cdot R_{1ob})]$.

As shown in Fig. 2b, we found good fitting results for R_{1ob} up to 8 s^{-1} with a pair of M_o* and TR*. Using this relationship, T_1-weighted image intensities were converted into the T_1 relaxation rates, as shown in Fig. 2c.

Estimation of simple diffusion of manganese in the brain

Based on the assumption of a simple diffusion of manganese in the brain, the increase in the T_1-relaxation rate ($\Delta R_1(x,t)$) was fitted to Eq. 5 with an offset of the diffusion axis (x_{off}).

$$\Delta R_1(x,t) = \Delta R_{10} \cdot \mathrm{erfc}[(x - x_{off})/(2(D_{ap} \cdot t)^{0.5})] \quad (6)$$

This technical offset was introduced to eliminate the uncertainty of the position of the 3V, since the thickness of the 3V is thinner than the pixel size (195 µm). The results shown from fitting 7 pixels from 195 to 1367 µm with a single diffusion coefficient (D_{ap}) are shown in Fig. 2d. Results obtained from 4 different rats showed good reproducibility: mean and SE of D_{ap} and x_{off} were $4.18 \pm 0.32 \times 10^{-5}$ mm^2 s^{-1} and 4.6 ± 3.5 µm, respectively. This D_{ap} value is much smaller than the water diffusion in the hypothalamus ($6.1 \pm 0.23 \times 10^{-4}$ mm^2 s^{-1}, $n = 4$). In addition, as shown in Fig. 2d, regression lines

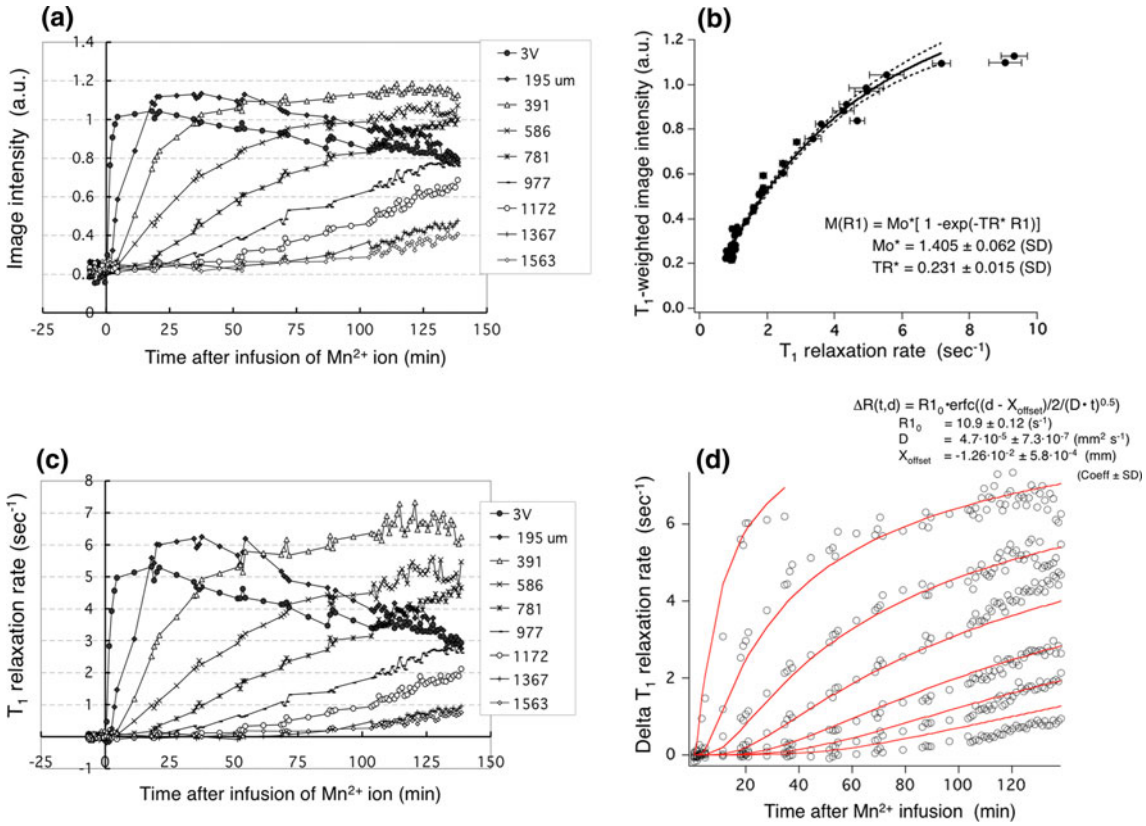

Fig. 2 Diffusion of Mn^{2+} in the rat brain from the 3rd ventricle. **a** Changes in image intensity of 9 pixels after the intraventricular infusion of 2 mM Mn-bicine (50 µl/h). The distance from the center of the pixel to the 3rd ventricle is shown in the legend for each of the pixels. **b** The relationship between the T_1 relaxation rate (R_{1ob}) and image intensity (M_{ob}). The *bold* and *dotted lines* represent, respectively, the regression line of the non-linear fitting and its 95% confidence range of image intensity to an equation: $M_{ob} = M_o^*[1 - \exp(-TR^* \cdot R_{1ob})]$, where M_o^* and TR* are apparent values of the equilibrium image intensity and the repetition time of the excitation pulse. Please refer to the text for the details. **c** Changes in the T_1 relaxation rate of 9 pixels after the intraventricular infusion of Mn-bicine. T_1 relaxation rates were calculated from the image intensity shown in **b** and the relationship obtained in **c**. **d** Fitting data for 7 pixels (195–1367 µm from the 3rd ventricle) to a simple one-dimensional diffusion equation with a single diffusion coefficient. The *bold lines* show results of fitting to $\Delta R_1(x,t) = \Delta R_{10} \cdot \mathrm{erfc}[(x - x_{off})/(2(D \cdot t)^{0.5})]$, where $\Delta R_{10} = 10.9 \pm 0.12\ s^{-1}$, $D = 4.7 \times 10^{-5} \pm 7.3 \times 10^{-7}\ mm^2\ s^{-1}$, $x_{off} = -1.26 \times 10^{-2} \pm 5.8 \times 10^{-4}$ mm (coefficient ± SD)

represented a systemic bias: regression lines moved to a value higher than the actual value when the distance from the 3V increased. Nonlinear fitting was applied to each of the pixels using the simple one-dimensional diffusion equation, Eq. (6). The results of the fitting are shown in Fig. 3a. Compared with Fig. 2d, the regression lines were overlapped exactly on the actual data. Means and SE of D_{ap} of 4 rats are shown in Fig. 3b. A significant difference ($p < 0.05$) was detected between the regression lines by one-way analysis of variance with distance from the 3V as a factor. Therefore, the diffusion of manganese in the 8 pixels was not a single simple diffusion process.

Discussion

Since manganese is an essential trace element for the brain and an excess of manganese is a neurotoxicant, many studies have been conducted on manganese uptake and efflux in the brain [9, 12, 13]. The transportation of manganese was usually estimated from the tissue concentration of manganese or by comparison of the concentration ratio in the brain to that in plasma. These studies focused on manganese transporters in the blood-brain barrier (BBB) and the blood-CSF barrier, and considered the brain parenchyma as a uniform single compartment. When we first began to employ manganese ion-enhanced MRI, we had to wait for a while for the interstitial diffusion of manganese. This interstitial diffusion seemed to be much slower than what we expected from the diffusion of the small Mn^{2+} ion, suggesting that not only the blood endothelium, but also brain parenchyma may hinder the lateral diffusion of manganese. As far as I can determine, no other reports concerning the interstitial transport of manganese in the brain have been published.

We measured the lateral diffusion of manganese from the 3V to the hypothalamus. The concentration of

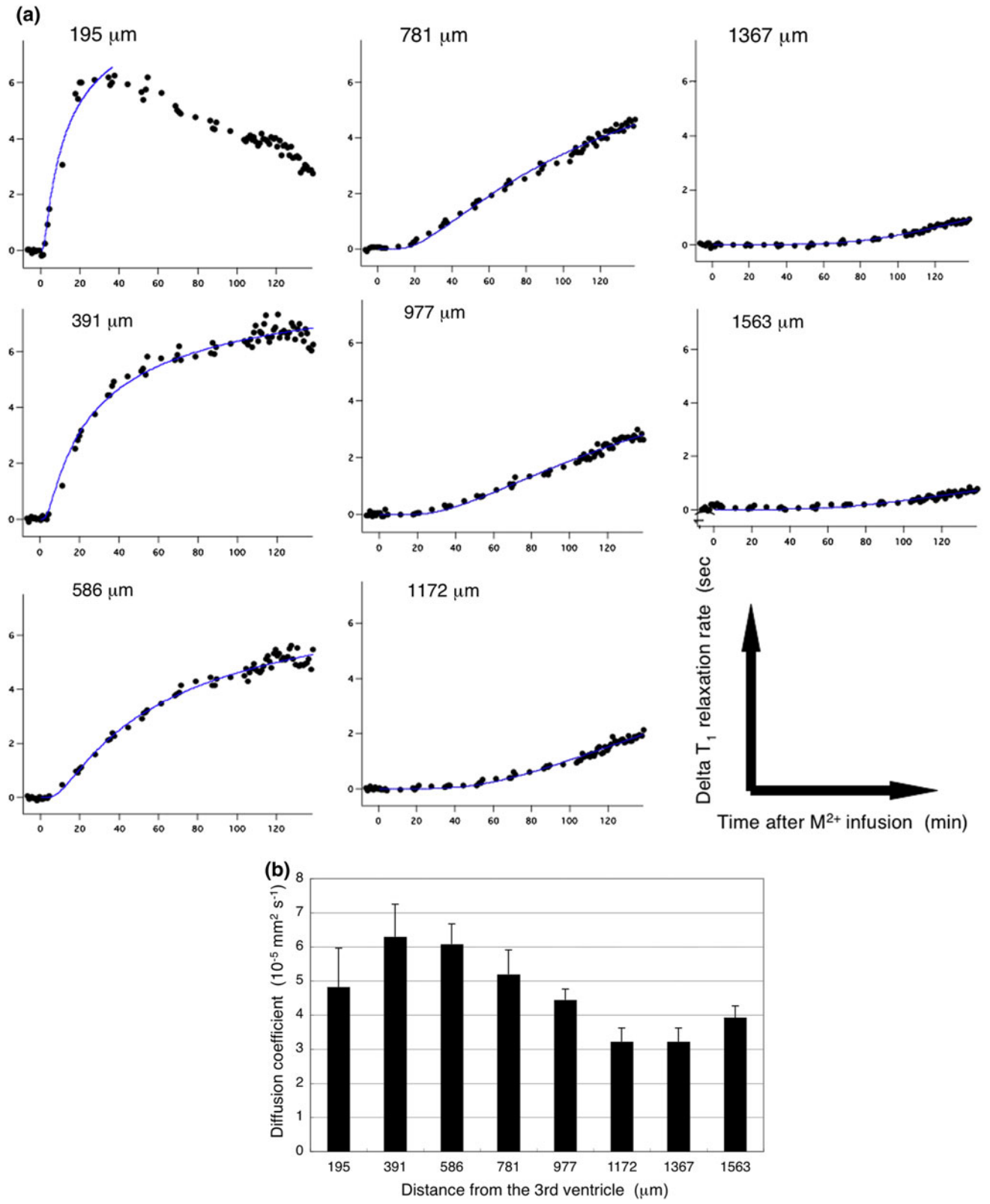

Fig. 3 Fitting the data for each pixel to a simple one-dimensional diffusion equation. **a** The *bold lines* show the results of the fitting. In regard to the pixel at 195 μm, fitting was performed using the data obtained in the initial 35 min. For the rest of the pixels, all data were used for the fittings. **b** Apparent diffusion coefficients for each pixel. Means and SE of 4 rats are shown. A significant difference ($p < 0.05$) between the coefficients was detected by one-way analysis of variance with distance from the 3rd ventricle as a factor

manganese was estimated from the T_1 relaxation rate estimated from the intensity of the T_1-weighted MR image. The observed apparent diffusion constant (D_{ap}) of manganese (4.2×10^{-5} mm^2 s^{-1}) was much smaller than that of water in the hypothalamus (ca. 6×10^{-4} mm^2 s^{-1}). From the Stokes-Einstein equation, the diffusion coefficient may scale as the inverse of the radius of molecule (r), i.e., the cube root of the molecular weight (m),

$$D = \mathrm{kT} \cdot (6\pi\eta\rho)^{-1} \propto r^{-1} \propto m^{(-1/3)},$$

where η is viscosity. This relationship was confirmed in a wide range of molecules from 170 to 10 kDa in the cytoplasm [14]. The D_{ap} value of manganese, 4.2×10^{-5} mm^2 s^{-1}, is comparable to that of 3–4 kDa molecular weight, which is much larger than the molecular weight of Mn^{2+} (55 Da), Mn-bicine (216 Da), Mn-citrate (245 Da), and $Mn(HCO_3)^+$ (116 Da). Serum albumin (66 kDa) does not cross the intact BBB, and the concentration of Mn transferrin (77 kDa) in brain extracellular fluid is less than 0.25 μM [9]. The contribution of these macromolecules can thus be ignored. Therefore, the slow diffusion of manganese could not be explained by molecular size. This is one reason why we did not focus on the different Mn species, but rather dealt with diffusion as single component.

The very slow diffusion of manganese might be explained by the intracellular deposition of Mn^{2+}. In normal conditions, the brain takes up Mn^{2+} by carrier-mediated processes, and most Mn^{2+} ions are chelated by citrate in the extracellular space of the brain [8, 9]. Based on their molecular size, Mn-citrate and Mn-bicine may not enter the cells themselves. From the literature, the conditional association constants of Mn-citrate (3.9 M^{-1}) and Mn-bicine (2.9 M^{-1}) are low [9, 15], and the association constant of $Mn(HCO_3)^+$ (1.2 M^{-1}) [16] is very low, and some fractions of Mn complexes dissociate free Mn^{2+} ions. The Mn^{2+} ion can enter neuronal cells through Ca^{2+} entry pathways, such as voltage-dependent Ca^{2+} channels. On the other hand, Mn^{2+} efflux might be a slow diffusion-mediated pathway [9, 13]. Therefore, Mn^{2+} ions tend to accumulate in the cells, so the D_{ap} of Mn^{2+} will become much slower than that expected from the molecular weight. It might also be true that there is some amount of manganese efflux from the brain via the veins. Indeed, as shown in Fig. 1d, a small vein crossed the pixel around 1000 μm from the 3V. That pixel position was close to the one that showed the lowest D_{ap} (Fig. 3b).

In regard to MnEMRI, we obtained useful experimental information employing the intraventricular application of Mn^{2+}. As shown in Fig. 2b, a range of $1/T_1$ from 1 to 5 s^{-1} is a suitable range of T_1 for MnEMRI. As shown in Fig. 2c, manganese can diffuse within 30 min in the regions 0–400 μm apart from the ventricles. Therefore, we can use a lower concentration of Mn^{2+} (e.g., 0.5 mM) for MnEMRI. On the other hand, in the regions around 1000 μm apart from the ventricles, we may have to wait for 1 h for the entry of Mn^{2+}, and we thus recommend a higher concentration of Mn^{2+} (e.g., 2–5 mM). It might be appropriate to mention the systemic application of Mn^{2+} in this regard. When Mn^{2+} is applied intravenously or intraperitoneally, the cerebral capillary and the choroid plexus are known to be the two main pathways for Mn^{2+} entry into the brain parenchyma. The uptake into the brain parenchyma via the choroid plexus becomes the predominant form [12]. Mn-bicine is also small enough to pass through the choroid plexus into the CSF, where it can then diffuse into the brain through the ependymal layer. Therefore, manganese diffusion from the cerebroventricles is an important route for Mn^{2+} entry even when employing the systemic administration of manganese. When manganese was infused intravenously for 1 h at a rate of 8.3 μmol kg^{-1} min^{-1}, the final plasma concentration of Mn^{2+} reached a value of about 0.5 mM [1, 6]. Then, the manganese passed through the choroid plexus into the CSF. The concentration of Mn^{2+} in the CSF might also increase to about 0.5 mM, which would be sufficient for the detection of the neural activities of the periventricular nuclei without breaking the BBB.

Acknowledgments The authors would like to thank Mr. S. Sato, Mr. H. Okawara (National Institute for Physiological Sciences), Ms. Y. Imaizumi, and Ms. M. Yokoi (Dokkyo Medical University School of Medicine) for their technical assistance. This study was supported by grants from the Ministry of Education, Science, and Culture of Japan, and the General Collaborative Project of National Institute for Physiological Sciences.

References

1. Lin YJ, Koretsky AP (1997) Manganese ion enhances T_1-weighted MRI during brain activation: an approach to direct imaging of brain function. Magn Reson Med 38:378–388
2. Morita H, Ogino T, Seo Y, Fujiki N, Tanaka K, Takamata A, Murakami M (2002) Detection of hypothalamic activation by manganese ion contrasted T_1-weighted magnetic resonance imaging. Neurosci Lett 326:101–104
3. Morita H, Ogino T, Fujiki N, Tanaka K, Gotoh TM, Seo Y, Takamata A, Nakamura S, Murakami M (2004) Sequence of forebrain activation induced by intraventricular injection of hypertonic NaCl detected by Mn^{2+} contrasted T_1-weighted MRI. Auton Neurosci 113:43–54
4. Silva AC, Lee JH, Aoki I, Koretsky AP (2004) Manganese-enhanced magnetic resonance imaging (MEMRI): methodological and practical considerations. NMR Biomed 17:532–543
5. Silva AC, Bock NA (2008) Manganese-enhanced MRI: an exceptional tool in translational neuroimaging. Schizophr Bull 34:595–604
6. Seo Y, Satoh K, Watanabe K, Morita H, Takamata A, Ogino T, Murakami M (2011) Mn-bicine: a low affinity chelate for manganese ion enhanced MRI. Magn Reson Med 65:1005–1012
7. Johanson CE (2008) The choroid plexus-cerebrospinal fluid circulatory dynamics: impact on brain growth, metabolism, and

repair. In: Conn MP (ed) Neuroscience in Medicine, 3rd edn, Humana Press, Totowa
8. Michalke B, Berthele A, Mistriotis P, Ochsenkühn-Petropoulou M, Halbach S (2007) Manganese species from human serum, cerebrospinal fluid analyzed by size exclusion chromatography-, capillary electrophoresis coupled to inductively coupled plasma mass spectrometry. J Trace Elem Med Biol 21(Suppl 1):4–9
9. Yokel RA (2009) Manganese flux across the blood–brain barrier. Neuromol Med 11:297–310
10. Seo Y, Takamata A, Ogino T, Morita H, Nakamura S, Murakami M (2002) Water permeability of capillaries in the subfornical organ of rats determined by Gd-DTPA^{2-} enhanced ^{1}H magnetic resonance imaging. J Physiol 545:217–228
11. Takamata A, Seo Y, Ogino T, Tanaka K, Fujiki N, Morita H, Murakami M (2001) Effects of pCO_2 on the CSF turnover rate in T_1-weighted magnetic resonance imaging. Jpn J Physiol 51:555–562
12. Aschner M, Guilarte TR, Schneider JS, Zheng W (2007) Manganese: recent advances in understanding its transport and neurotoxicity. Toxicol Appl Pharmacol 221:131–147
13. Crossgrove J, Zheng W (2004) Manganese toxicity upon overexposure. NMR Biomed 17:544–553
14. Mastro AM, Keith AD (1984) Diffusion in the aqueous compartment. J Cell Biol 99:180s–187s
15. Chelating Agents (2008). In products catalog 26th edit. Kumamoto: Dojindo Laboratories. p 307–322 (in Japanese)
16. Lesht D, Bauman JE Jr (1978) Thermodynamics of the manganese(II) bicarbonate system. Inorg Chem 17:3332–3334